RADIO-ECHO SOUNDING DETERMINATION OF POLYTHERMAL GLACIER HYDROLOGY

Luke Copland and Martin Sharp
University of Alberta
Department of Earth and Atmospheric Sciences, Edmonton, Alberta T6G 2E3, Canada
luke.copland@ualberta.ca martin.sharp@ualberta.ca

ABSTRACT

In this paper we describe three sources of information that radio-echo sounding has provided about the subsurface hydrology of a polythermal glacier:

1. **Water input locations:** crevasses and moulins provide the main pathway for surface melt to reach the interior of the glacier, and are identifiable as strong reflectors close to the glacier surface.
2. **Subglacial flow routing:** common mid-point surveys are used to calculate the radio-wave velocity through the glacier. Reflections from the glacier bed are then converted to ice depths, which are subtracted from the surface topography to determine bed topography. These are used to reconstruct the subglacial hydraulic potential surface and likely patterns of basal water flow.
3. **Subglacial properties:** repeat surveys at the same location over 9 days display diurnal variations and changes in bed reflection power associated with changes in basal water flow.

Keywords: Polythermal glacier, arctic, Canada, hydrology, radio-echo sounding, radar, ice, water flow, Ellesmere Island

INTRODUCTION

Many studies have demonstrated that water at the bed of a glacier influences ice motion via the influence of subglacial water pressure on basal shear traction (Willis, 1995). Geomorphological evidence and computer models also indicate that subglacial hydrology was a crucial control on the dynamics of the Pleistocene mid-latitude ice sheets (Arnold and Sharp, 1992). High Arctic glaciers exhibit polythermal basal conditions which most closely resemble those found beneath Pleistocene ice sheets (Heine and McTigue, 1996), but little is currently known about their hydrology. Polythermal glaciers contain ice that is both at and below the pressure melting point, with high Arctic glaciers characterized by warm ice that is present only close to the glacier bed in the ablation area (Blatter and Hutter, 1991).

In **this paper** we discuss three sources of information which radio-echo sounding has provided about the subglacial hydrology of a polythermal glacier: the location of water input points to the glacier interior, the routing of water across the glacier bed, and temporal changes in basal water flow.

STUDY SITE

John Evans Glacier is a polythermal valley glacier on the east coast of Ellesmere Island, Nunavut, Canada (79°40'N, 74°30'W; Figure 1). It covers an area of approximately 165 km^2, and ranges in elevation from 100 m to 1200 m asl. Mean annual air temperature is -14.7°C over the glacier terminus. High bed reflection powers and the presence of an internal reflector in radio-echo sounding records indicate a warm base beneath most of the ablation zone (Copland and Sharp, in review).

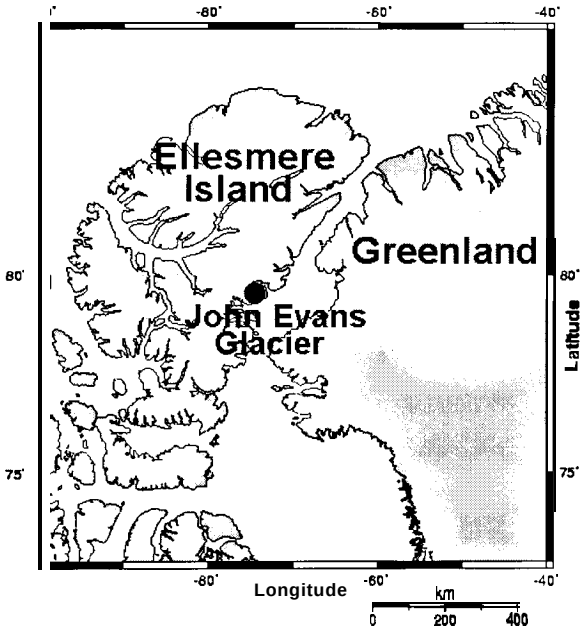

Figure 1: Location of John Evans Glacier

Radio-echo sounding measurements were made at ~3200 locations over the glacier surface with a custom-built unit

operating at centre frequencies of 5, 10 or 20 MHz (higher frequencies were used in shallower ice depths). The monopulse transmitter produced a peak power of 24 kW (Narod and Clarke, 1994), and a Tektronix 730 digital oscilloscope connected to a HP palmtop computer acted as the receiver and data recorder. The unit was towed on two sleds, and the signal was low pass filtered at 1.5x the transmitted centre frequency and averaged over 32 traces to reduce noise. It was then high pass filtered to remove the WOW with the RADAN software package (Geophysical Survey Systems, Inc.). The data were not migrated due to irregular trace and transect spacing caused by complex surface topography, crevasses, and deeply incised surface streams.

RESULTS

Water input locations

For most polythermal glaciers, crevasses (linear cracks in the ice surface) and moulins (near-vertical shafts) provide the main routes for water to enter the glacier interior. The location and characteristics of these features is an important input for hydrological modelling because they control the subglacial water distribution, which in turn is a control on ice dynamics. They can be observed where the snow melts in the summer, but are difficult to map in other parts of the glacier and at other times of the year.

Crevasses and moulins are identifiable in radio-echo sounding records as a series of near-surface reflectors due to the large dielectric contrast between glacier ice and the air or water within them. There are few other internal reflectors in polythermal glaciers, so plots of spatial variability in internal reflection power (IRP) provided an effective means of identifying these features. Returned power was determined by squaring the amplitudes of the raw traces, with the IRP calculations covering the period between the end of the ground wave and the start of the bed reflection. To normalize the results, the total power was divided by the measurement period to produce units of mv^2/ns.

Figure 2 shows the variability in IRP over John Evans Glacier, and there is indeed a strong correlation between areas of high IRP and the location of crevasses and moulins seen in the field and in aerial photos.

Subglacial flow routing

Raw radio-echo sounding data provide basic information about the shape and relative location of reflectors, but little about their actual depth below the surface unless the radio wave velocity (RWV) is known. The RWV in a glacier depends on many factors such as ice density, water content

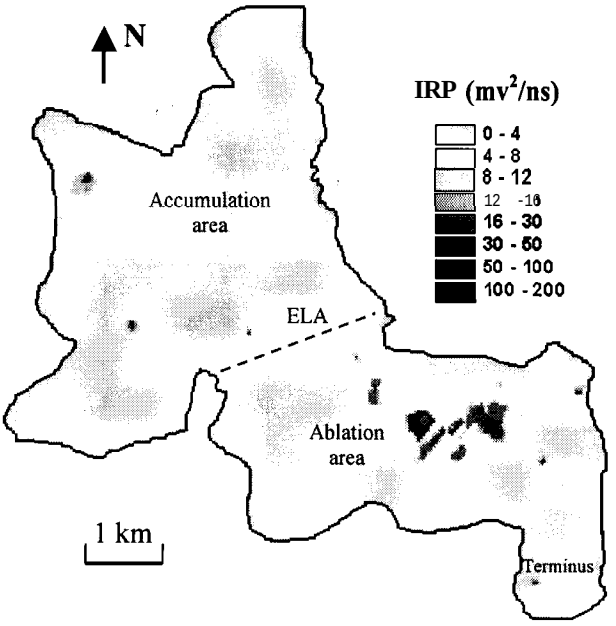

Figure 2: Variability in internal reflection power (IRP) over John Evans Glacier. High values correlate with the location of crevasses and moulins. ELA = Equilibrium line altitude.

and ice structure, with measured values typically in the range 0.150 to 0.190 m ns^{-1} (Bogorodsky et al., 1983). Many workers use a mean velocity of 0.167 m ns^{-1} to convert travel times to depths (e.g., Knudsen & Hasholt, 1999), but this value is not appropriate for all glaciers.

To determine the appropriate RWV for John Evans Glacier, a series of common mid-point (CMP) soundings were made at 12 locations over the glacier surface in summer 1999. CMP surveys involve separating the transmitter and receiver equally from a central point while measuring the variation in travel time of the waves to a central bed reflector. An example of the results from such a survey are provided in Figure 3, with the three primary radar returns relating to:

1. The air wave (A) - which triggers the oscilloscope, and travels directly through the air between the transmitter and receiver at the speed of light (-0.300 m ns^{-1})
2. The ground wave (G) - which travels along the near surface at the RWV of ice.
3. The bed wave (B) - which is reflected from the glacier bed and travels at the RWV of ice.

The RWV of ice is determined by solving (Macheret et al., 1993):

$$\tau_B = 1/V_B \sqrt{(4h_B^2 + d^2 \cos^2 \alpha_B)} \qquad (1)$$

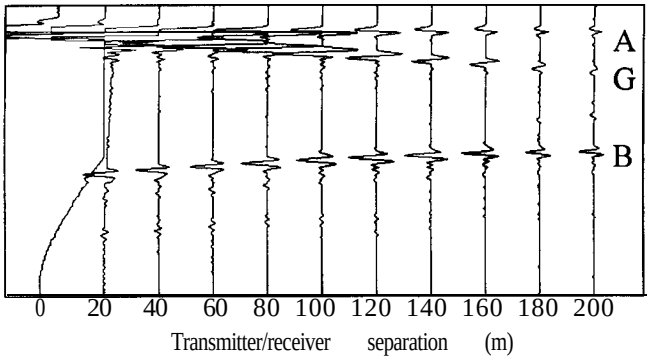

Figure 3: An example set of traces from a common mid-point survey at John Evans Glacier. A = air wave; G = ground wave; B = bed wave. Depth to bed is -124 m.

where $\tau_B = \tau_d + \tau_0$ (τ_d is the delay time of the bottom signal B measured relative to A, τ_0 is the propagation time in air of signal A from the transmitter to the receiver), V_B is the mean velocity of the bottom signal B, ha is the echo depth of the bottom, d is the antenna separation distance, and α_B is the difference in slope angles of the glacier surface and glacier bed. Given that α_B is approximately 0 at the CMP locations, Equation (1) can be transformed to a linear form:

$$y = a x + b \qquad (2)$$

by squaring and assigning:

$$y = \tau_B^2,\ x = d^2,\ a = 1/V_B^2,\ b = 4h_B^2/V_B^2 \qquad (3)$$

the RWV through the ice is calculated by plotting d^2 vs. τ_B^2, and fitting a linear least-squares regression line through the data points (Figure 4). The mean velocity is then given by the slope of the regression line. For the 12 CMP sites on John Evans Glacier, the mean RWV was 0.17 11 m ns^{-1}, with a standard deviation of 0.0031 m ns^{-1}. This velocity is equivalent to a real dielectric constant of 3.074. Using this velocity (V,,,), the ice depth (h) was determined for the 3200 trace locations at John Evans Glacier by:

$$h = (t_s + t_b)/2 * V_{ice} \qquad (4)$$

where t_s is the time taken for the trigger wave to pass across the glacier surface between the transmitter and receiver, and t_b is the time between the peak of the surface and bed waves. The times are halved to convert the two-way travel time to an ice depth.

A digital elevation model (DEM) of the glacier bed was produced by subtracting the ice depth from the surface elevation and then interpolating between the known bed elevations with a TIN (triangular irregular network). The horizontal location of each trace was measured with a hand-held GPS, and the surface elevation was determined by referencing the horizontal location to a DEM of the glacier surface derived from aerial photogrammetry (Woodward et al., 1997). Both the surface and bed DEMs were interpolated to matching 25 m grids.

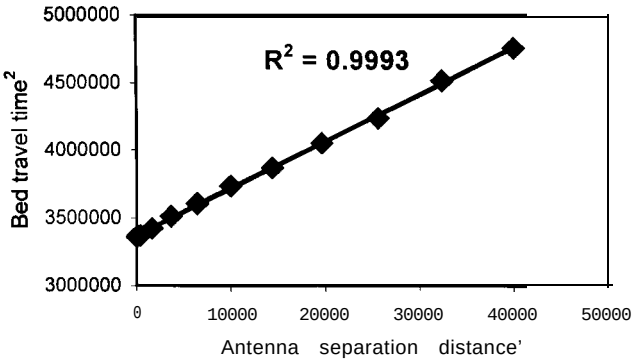

Figure 4: An example of the linear regression used to calculate the mean radio wave velocity through ice at John Evans Glacier. R^2 values were >99.99% significant for all 12 common mid-point surveys.

Using a modification of the method outlined by Shreve (1972), the gridded hydraulic potential was calculated from the DEMs of the glacier surface and bed by (Paterson, 1994):

$$\Phi = \rho_w g B + f \rho_i g (H - B) \qquad (5)$$

where ρ_w and ρ_i are the densities of water and ice, g is the acceleration due to gravity, B is the bed elevation, f is the subglacial water pressure as a fraction of ice overburden pressure (i.e., p_w/p_i), and H is the surface elevation. Using the 'hydro' extension in ArcView, the drainage reconstruction was produced from the gridded hydraulic potentials in three steps:

1. Any sinks (i.e., overdeepenings) were tilled to allow water to pass across them
2. The flow direction was defined by the adjacent cell with the lowest elevation
3. The flow accumulation was calculated as the number of upstream cells that flow into each downslope cell

Figure 5 shows the reconstructed subglacial drainage for the ablation area of John Evans Glacier for f = 1, and for cells with upstream flow accumulation of 50 cells or more. The reconstruction is not shown for the accumulation area due to the low bed reflection powers there that are indicative of cold-based ice and a dry bed (Copland and Sharp, in review). Reconstructions with different values off made no significant difference to the flow routing, and

increasing/decreasing the specified minimum flow accumulation simply shortened/lengthened the individual flow paths. A reconstruction of water flow over the bedrock under atmospheric conditions was also made (i.e., f = 0), but this made no significant difference to the routing.

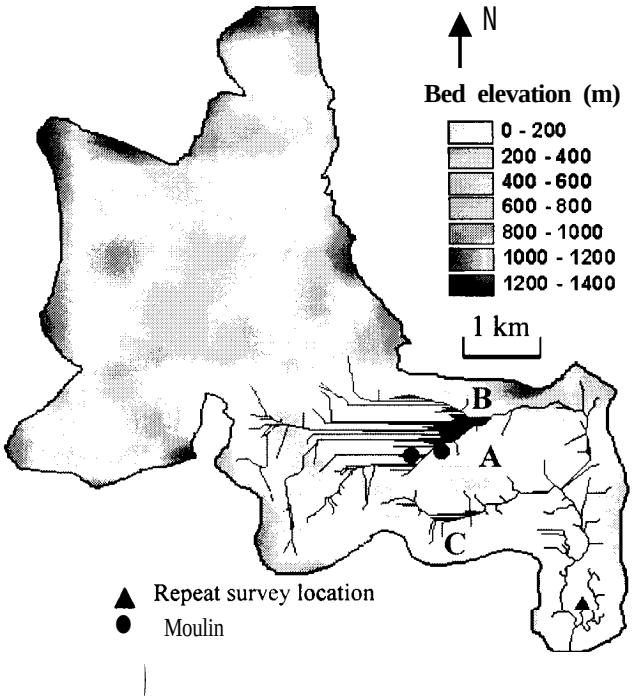

Figure 5: Subglacial flow reconstruction for the ablation area of John Evans Glacier. A is a bedrock ridge; B and C indicate overdeepened areas and separate catchments.

From these reconstructions, it is evident that bedrock topography dominates flow routing beneath John Evans Glacier. A large bedrock ridge (A in Figure 5) controls flow in the ablation area, with most water flowing in the catchment to the north of the ridge (B) before reaching the glacier terminus. There is a secondary catchment (C) to the south of the bedrock bump with a smaller upstream accumulation area. There are also overdeepened areas to the north and south of the bedrock ridge where the flow reconstructions suggest that water collects (B and C in Figure 5). Further evidence for subglacial water ponding in these areas is provided by the presence of high bed reflection powers (Copland and Sharp, in review).

The black dots in Figure 5 mark the location of two large moulins in the area of high IRPs (Figure 2), which provide sinks for supraglacial streams. If water reached the glacier bed directly beneath these features it would flow in the northern catchment, although it could pass into the southern catchment as observations suggest that water may flow for considerable distances englacially between the base of moulins and the glacier bed (Holmlund, 1988). Further work (e.g., dye tracing) is necessary to determine which routing is correct.

Subglacial properties

Repeat traces at the same location in the centre of the glacier terminus were recorded over a nine day period in July 1999 (the survey location is marked by a triangle in Figure 5). The system parameters remained the same for all surveys, with a transmitted centre frequency of 10 MHz, a parallel antenna configuration with the dipoles aligned up- and down-glacier, and a receiver/transmitter separation of 10 m. Ice depth at the measurement location was 124 m.

The timing of the bed reflection was the same for all traces, but its strength varied greatly (Figure 6a). Since the system setup and ice depth remained constant, it is assumed that variability in bed reflection power is related to differences in transmitted energy and/or the nature of the basal reflector. Gades (1998) argued that variable coupling between the antennae and glacier surface can produce significant differences in the amount of power transmitted into the glacier, and is primarily influenced by the amount of water at the glacier surface. More water results in better coupling and stronger basal reflection strengths, even when conditions at the glacier bed are constant. To determine the variability in surface coupling at John Evans Glacier, the ground wave power was determined for all repeat traces. If surface coupling is an influence on basal reflection strength, there should be a positive relationship between bed power and ground wave power. Figure 7 shows that such a relationship does not exist, however, which suggests that variability in basal reflection strength is related to physical changes at the glacier bed.

There are two notable patterns in bed reflection power: there are marked diurnal variations over the first two days when measurements were made twice a day, and there is a general decrease towards the end of the survey period (Figure 6a). Gauging records from a supraglacial stream which feeds water to the glacier bed via one of the moulins marked on Figure 5, and from a proglacial stream that provides the main outflow at the glacier terminus (Figure 6b), and air temperature records from a weather station -250 m upglacier of the survey point (Figure 6c), display several similarities to the bed power patterns.

The diurnal variations in bed power on Julian Day (JD) 190 and 191 correlate closely with supraglacial stream discharge during a period of relatively warm weather, with powers higher in the late afternoon than the morning. In addition, the higher diurnal bed powers on JD 191 than JD 190 correlate with an increase in proglacial discharge over this time. This proglacial discharge event represents the flood

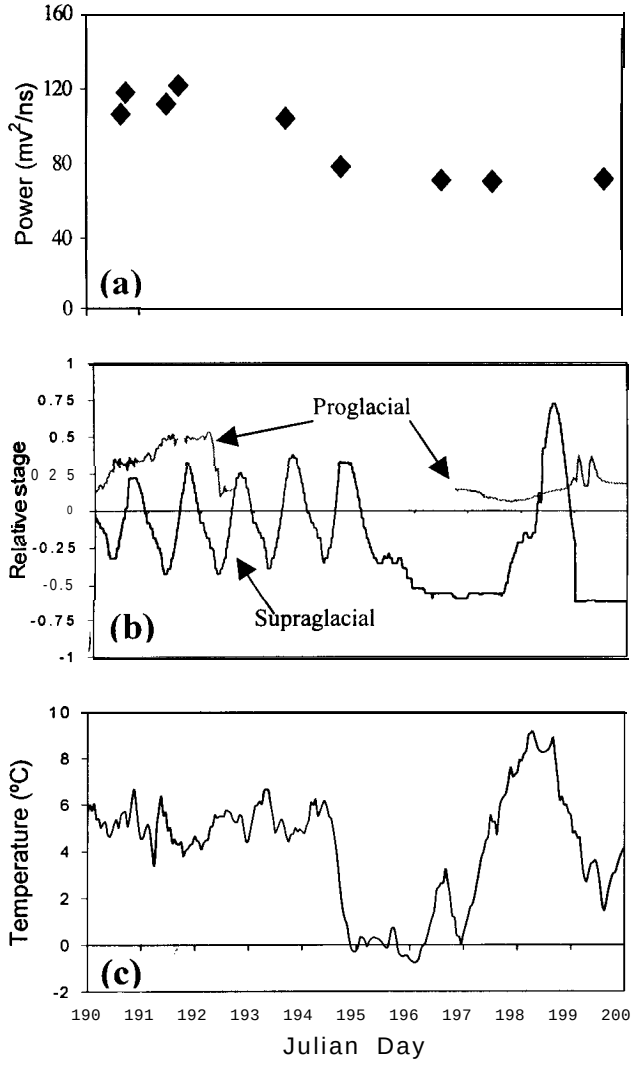

Figure 6 (a) Variability in bed reflection power over the repeat survey period (Julian Day 190 = July 9, 1999). (b) Supraglacial and proglacial stream stage records. Part of the proglacial stream record is missing due to changes in the location of the main channel (c) Air temperature recorded at a weather station on the glacier terminus.

generated by drainage of a supraglacial lake into one of the moulins identified in Figure 5 on JD 188. Proglacial discharge then falls on JD 193 as the glacier bed dries out, with a decrease in supraglacial discharge and virtual disappearance of diurnal patterns after JD 195 as the weather cools and there is a small snowfall. Bed power also declines over this period, with values during the coldest and lowest discharge period on JD 196 and 197 almost half of those at the peak on JD 19 1. The supraglacial, and later the proglacial, discharge increases on JD 198 and the early part of JD 199 as the weather warms, but then falls again on JD 199 as temperatures cool. By the time a radar measurement

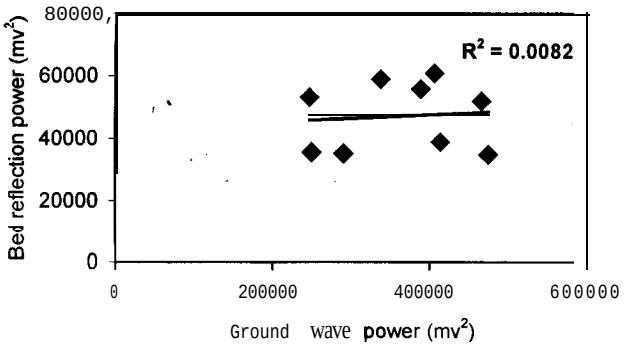

Figure 7: Relationship between ground wave power and bed reflection power for the repeat surveys.

was made late in the day on JD 199 the water had largely drained from beneath the glacier terminus, and consequently the bed power remained low.

From these records, it appears that variability in the quantity of water at the glacier bed is the dominant control on returned bed power. This is explained by the dielectric constant of water, which is approximately four times higher than any other subglacial material.

Figure 5 shows that the repeat survey point is located at the upper end of a predicted subglacial flow path, which suggests that variability in bed power might arise from changes in water flow through a subglacial channel. If this was the case, a phase inversion would be expected in radio-echo sounding returns as the channel filled and drained because the dielectric constant of air is lower than that of ice, while the dielectric constant of water is higher than that of ice (Arcone, 1996). The phase remains constant for all traces, however, which makes it likely that the radar returns are responding to changes in water flow through or over basal sediment. A 4 m thick aquifer beneath the glacier snout provides strong support for a sediment layer beneath the terminus region (Skidmore and Sharp, 1999), and Gades (1998) demonstrates that bed power changes of 25-50% can be produced on the time scale of days by changes in porosity and/or water conductivity in the upper portion of a stratified till layer.

CONCLUSIONS

This study has demonstrated that radio-echo sounding provides an effective method for monitoring and detecting several hydrological features of polythermal glaciers:

1. Internal and near-surface features such as moulins and crevasses can be identified by high internal reflection powers. This provides a method for remotely mapping

near-surface features which are often snow covered and difficult to access in the field.

2. Using common mid-point surveys, the mean radio-wave velocity through John Evans Glacier was measured as 0.1711 ± 0.003 1 m ns^{-1}. This enables determination of true ice thickness and bed topography, and allows predictions of subglacial flow routing. These flow predictions are supported by maps of returned bed power (Copland and Sharp, in review).
3. Repeat traces over a 9 day period in July 1999 show strong relationships between basal reflection strength, air temperature, and supraglacial/proglacial stream discharge, and provide a method for monitoring changes in hydrological conditions at the glacier bed.

ACKNOWLEDGEMENTS

We would like to thank the Nunavut Research Institute for permission to work at John Evans Glacier, and the Natural Sciences and Engineering Research Council of Canada, Polar Continental Shelf Project (contribution number 00800), Geological Society of America, and the Canadian Circumpolar Institute of the University of Alberta for funding and field logistics. Anthony Arendt, James Davis, Wendy Davis, Darek Glowacki, Trudy Wohlleben and Peter Nienow were of great help in the field.

REFERENCES

Arcone, S.A. 1996. High resolution glacial ice stratigraphy: a ground-penetrating radar study of Pegasus Runway, McMurdo Station, Antarctica. *Geophysics,* Vol. 6 1, pp. 1653-1663.

Arnold, N. and Sharp, M. 1992. Influence of glacier hydrology on the dynamics of a large Quaternary ice sheet. *Journal of Quaternary Science,* Vol. 7, pp. 109-124.

Blatter, H. and Hutter, K. 199 1. Polythermal conditions in Arctic glaciers. *Journal of Glaciology,* Vol. 37, pp. 261-269.

Bogorodsky, V., Bentley, C. and Gudmandsen, P. 1983. *Radioglaciology.* Reidel, Dordrecht, 254 pp.

Copland, L. and Sharp, M. *In review.* Mapping hydrological conditions beneath a polythermal glacier using radio-echo sounding. *Journal of Glaciology.*

Gades, A.M. 1998. Spatial and temporal variations of basal conditions beneath glaciers and ice sheets inferred from radio echo-sounding measurements. Unpublished Ph.D. thesis, University of Washington.

Heine, J.T. and McTigue, D.F. 1996. A case for cold-based continental ice sheets – a transient thermal model. *Journal of Glaciology,* Vol. 42, pp. 37-42.

Holmlund, P. 1988. Internal geometry and evolution of moulins, Storlgaciaren. Sweden. *Journal of Glaciology,* Vol. 34, pp. 242-248.

Knudsen, N.T. and Hasholt, B. 1999. Radio-echo sounding at the Mittivakkat Gletscher, Southeast Greenland. *Arctic, Antarctic and Alpine Research,* Vol. 3 1, pp. 321-328.

Macheret, Y.Y., Moskalevsky, M.Y. and Vasilenko, E.V. 1993. Velocity of radio waves in glaciers as an indicator of their hydrothermal state, structure and regime. *Journal of Glaciology,* Vol. 39, pp. 373-384.

Narod, B.B. and Clarke, G.K.C. 1994. Miniature high-power impulse transmitter for radio-echo sounding. *Journal of Glaciologv,* Vol. 40, pp. 190- 194.

Paterson, W.S.B. 1994. *The Physics of Glaciers* (3rd ed.). Elsevier Science, Oxford, 480 pp.

Shreve, R.L. 1972. Movement of water in glaciers. *Journal of Glaciology,* Vol. 11, pp. 205-214.

Skidmore, M.L. and Sharp, M.J. 1999. Drainage system behaviour of a High Arctic polythermal glacier. *Annals of Glaciologv,* Vol. 28, pp. 209-215.

Willis, I.C. 1995. Intra-annual variations in glacier motion: a review. *Progress in Physical Geography,* Vol. 19, pp. 61-106.

Woodward, J., Sharp, M. and Arendt, A. 1997. The effect of superimposed ice formation on the sensitivity of glacier mass balance to climate change. *Annals of Glaciology,* Vol. 24, pp. 186-190.